Spatial Correspondence Between Intraretinal Fluid, Subretinal Fluid, and Pigment Epithelial Detachment in Neovascular Age-Related Macular Degeneration

Sophie Klimscha,[1] Sebastian M. Waldstein,[1] Thomas Schlegl,[1] Hrvoje Bogunović,[1] Amir Sadeghipour,[1] Ana-Maria Philip,[1] Dominika Podkowinski,[1] Eleonore Pablik,[2] Li Zhang,[3] Michael D. Abramoff,[3] Milan Sonka,[3] Bianca S. Gerendas,[1] and Ursula Schmidt-Erfurth[1]

[1]Christian Doppler Laboratory for Ophthalmic Image Analysis, Vienna Reading Center, Department of Ophthalmology and Optometry, Medical University of Vienna, Vienna, Austria
[2]Center for Medical Statistics, Informatics and Intelligent Systems, Medical University of Vienna, Vienna, Austria
[3]Department of Electrical and Computer Engineering, The University of Iowa, Iowa City, Iowa, United States

Correspondence: Ursula Schmidt-Erfurth, Department of Ophthalmology, Medical University of Vienna, Spitalgasse 23, 1090 Vienna, Austria; ursula.schmidt-erfurth@meduniwien.ac.at.

Submitted: June 27, 2016
Accepted: June 5, 2017

Citation: Klimscha S, Waldstein SM, Schlegl T, et al. Spatial correspondence between intraretinal fluid, subretinal fluid, and pigment epithelial detachment in neovascular age-related macular degeneration. *Invest Ophthalmol Vis Sci*. 2017;58:4039–4048. DOI:10.1167/iovs.16-20201

Purpose. To identify the spatial distribution of exudative features of choroidal neovascularization in neovascular age-related macular degeneration (nAMD) based on the localization of intraretinal cystoid fluid (IRC), subretinal fluid (SRF), and pigment-epithelial detachment (PED).

Methods. This retrospective cross-sectional study included spectral-domain optical coherence tomography volume scans (6 × 6 mm) of 1341 patients with treatment-naïve nAMD. IRC, SRF, and PED were detected on a per-voxel basis using fully automated segmentation algorithms. Two subsets of 37 volumes each were manually segmented to validate the automated results. The spatial correspondence of components was quantified by computing proportions of IRC-, SRF-, or PED-presenting A-scans simultaneously affected by the respective other pathomorphologic components on a per-patient basis. The median across the population is reported. Odds ratios between pairs of lesions were calculated and tested for significance pixel wise.

Results. Automated image segmentation was successful in 1182 optical coherence tomography volumes, yielding more than 61 million A-scans for analysis. Overall, 81% of eyes showed IRC, 95% showed SRF, and 92% showed PED. IRC-presenting A-scans also showed SRF in a median 2.5%, PED in 32.9%. Of the SRF-presenting A-scans, 0.3% demonstrated IRC, 1.4% PED. Of the PED-presenting A-scans, 5.2% contained IRC, 2.0% SRF. Similar patterns were observed in the manually segmented subsets and via pixel-wise odds ratio analysis.

Conclusions. Automated analyses of large-scale datasets in a cross-sectional study of 1182 patients with active treatment-naïve nAMD demonstrated low spatial correlation of SRF with IRC and PED in contrast to increased colocalization of IRC and PED. These morphological associations may contribute to our understanding of functional deficits in nAMD.

Keywords: optical coherence tomography, automated image analysis, age-related macular degeneration, intraretinal cystoid fluid, subretinal fluid

Age-related macular degeneration (AMD) leads to severe and irreversible vision loss, with an estimated prevalence of 8.7% worldwide.[1] Diagnosis and monitoring of AMD have been revolutionized by the introduction of optical coherence tomography (OCT) into disease management.[2] In state-of-the-art antivascular endothelial growth factor (anti-VEGF) therapy of neovascular AMD (nAMD), clinical practice and research rely on OCT to detect fluid pooling and degenerative changes.[3] In active nAMD disease, intraretinal cystoid fluid (IRC), subretinal fluid (SRF), and pigment epithelial detachment (PED) are the major pathomorphologic components on OCT considered relevant "imaging biomarkers" for visual function and for treatment indication.[4] Different predictive impacts on visual acuity attributed to these fluid compartments have been described at baseline as well as during the course of anti-VEGF therapy. Whereas IRC appears to be associated with poor visual outcomes, patients affected by SRF seem to have a more favorable visual prognosis.[5–9] Such findings concerning structure/function correlation of imaging biomarkers may be important for personalized treatment recommendations as well as future clinical trial designs.

Concerning the seemingly beneficial role of SRF, previous reports have suggested reduced rates of concomitant retinal pigment epithelial (RPE) atrophy and fibrosis over time[7,10] as well as reduced damage of outer retinal layers[11] (Philip A-M, et al. *IOVS* 2016;57:ARVO E-Abstract 4164) as responsible for its protective effect on visual function. Clinical observation suggests that retinal locations affected by SRF are less likely to exhibit simultaneous IRC, which may present a morphological condition conferring a protective effect particularly when SRF is located subfoveally. The aim of our study was to provide insight into the interplay between the individual fluid

compartments by analyzing the spatial correspondence of pathomorphological components in nAMD. We investigated the spatial overlap of IRC, SRF, and PED in spectral domain (SD)-OCT volumes in a large number of treatment-naïve eyes with nAMD. Automated three-dimensional segmentation of the pathomorphologic components was performed to precisely detect the presence and extent of IRC, SRF, and PED pooling. More than 60 million retinal locations of 1341 patients were tested in this "big data" approach for the co-occurrence of exudative features as a result of active choroidal neovascularization (CNV).

Methods

Study Population

This retrospective cross-sectional study was conducted in accordance with the Declaration of Helsinki and the International Conference of Harmonization of Good Clinical Practice guidelines. We included SD-OCT data of treatment-naïve patients with nAMD enrolled in prospective, randomized, multicenter clinical trials that were available at the Vienna Reading Center (VRC), that is, the HARBOR trial (clinicaltrials.gov identifier NCT00891735) and the OCTAVE trial (clinicaltrials.gov identifier NCT01780935). These trials had similar inclusion/exclusion criteria by protocol. For eligibility, patients had to present with treatment-naïve CNV secondary to AMD, as confirmed by fluorescein angiography, SD-OCT, and clinical examination by a retina specialist. Only one eye of each patient was included. Patients had to be aged 50 years or older and were eligible if the best-corrected visual acuity score was between 23 and 78 early-treatment diabetic retinopathy study letters (approximately 20/320-20/32 Snellen equivalent). Eyes showing central RPE atrophy or fibrosis were excluded. Only the treatment-naïve baseline visits were analyzed in this study. Furthermore, for validation purposes we included baseline Cirrus SD-OCT data of treatment-naïve nAMD patients enrolled in a single-center study at the Department of Ophthalmology at the Medical University of Vienna, for which manual annotations of IRC, SRF, and PED were available. This dataset was described in detail previously and had similar inclusion/exclusion criteria to the remaining dataset.[12] All patients provided written informed consent at the respective centers before enrollment into the clinical trials, and institutional review board approval was obtained at each participating center. All data were completely stripped from patient-identifying information before being entered into the image analysis database. Approval for the retrospective analysis was further obtained in advance from the Ethics Committee at the Medical University of Vienna.

Imaging

SD-OCT images were acquired by certified masked examiners, and raw data were uploaded to the VRC for analysis. Only eyes scanned using Spectralis OCT (Heidelberg Engineering, Heidelberg, Germany) or Cirrus HD-OCT (Carl Zeiss Meditec, Dublin, CA, USA) were included into the current analysis. With Spectralis OCT, volume scans of 512 A-scans by 49 B-scans covering a 6 × 6-mm area were used. With Cirrus HD-OCT, volume scans of 512 A-scans by 128 B-scans covering a 6 × 6-mm area were used.

Image Analysis

A fully automated image analysis pipeline established at the VRC was used to analyze all SD-OCT volumes. The retinal layers were segmented using the Iowa Reference Algorithms (Retinal Image Analysis Laboratory, Iowa Institute for Biomedical Imaging, Iowa City, IA, USA).[13] IRC and SRF were detected on a per-voxel basis using a fully automated machine learning algorithm based on convolutional neural networks. The algorithm and its accuracy have been validated previously.[14] PED was segmented using the Iowa Reference Algorithms based on a multiscale graph search method that fits surfaces to Bruch's membrane and the outer RPE boundary.[15,16] In a postprocessing step, we applied a previously described size definition for PED including only lesions of more than 400 μm width and 75 μm height or more than 200 μm height.[8] Segmentation of IRC and SRF requires delineation of retinal boundaries, defined as the internal limiting membrane and the RPE. Therefore, OCT volumes with an invalid layer segmentation did not enter the process of fluid segmentation and were excluded automatically. Layer segmentation was regarded as invalid if either negative values or a crossing of internal limiting membrane and RPE layers were generated.

To report spatial correspondence, the presence of IRC, SRF, and PED was assessed on a per A-scan level (vertical projection). Figure 1 illustrates an exemplary assessment of spatial correspondence. All analyses were performed on an area of 6 × 6 mm to provide sufficient evaluation of lesion extent. Furthermore, the central 1-mm area of the volume was analyzed separately to verify results in the area of greatest relevance for visual acuity. For this purpose, the center of the fovea was manually annotated by certified readers of the VRC.

In a subset of patients ($n = 37$) imaged by Cirrus, IRC and SRF had previously been manually annotated using a validated procedure as described in detail previously.[12] Furthermore, manual PED annotation, using the same width and height criteria as mentioned previously, was performed. Likewise, IRC, SRF, and PED were annotated in a subset ($n = 37$) imaged by Spectralis. These subsets of data served the purpose of validation.

Statistical Analysis

The dataset was analyzed using descriptive, mainly frequency, odds ratios (ORs) and chi-square statistics. Median and interquartile range (IQR) were used to describe data because of skewed distribution. Spatial correspondence was assessed by calculating the percentages of IRC-, SRF-, or PED-presenting A-scans also affected by one or both of the respective other pathomorphologic components on a per-patient base. We report the median percentages and IQR across the population. To rule out the possibility that these descriptive findings may be a result of inherent distribution characteristics of each pathomorphologic feature (e.g., median spatial correspondence of IRC and SRF is low because IRC a priori occurs in areas, where SRF occurs less likely and vice versa), per-pixel statistical analyses were performed for each pair of pathomorphologic components. ORs between the pairs were calculated for each pixel across all patients and the relationship was tested for significance using chi-square tests. The projected en-face area of the pathomorphologic components is reported as affected area in mm^2 and presented using the median and IQR of the area relative to the whole scan. Cases were included in the descriptive analyses if all pathomorphologic components under investigation were present. Analysis of spatial correspondence in the central 1-mm field required the basic component to be present in the central 1-mm field and the component investigated for being colocalized with the basic component to be present at least in the 6 × 6-mm field. To investigate the relation of presence and absence of IRC and SRF in the subfoveal area, a chi-square test of independence was performed. Cirrus and Spectralis scans were compared by

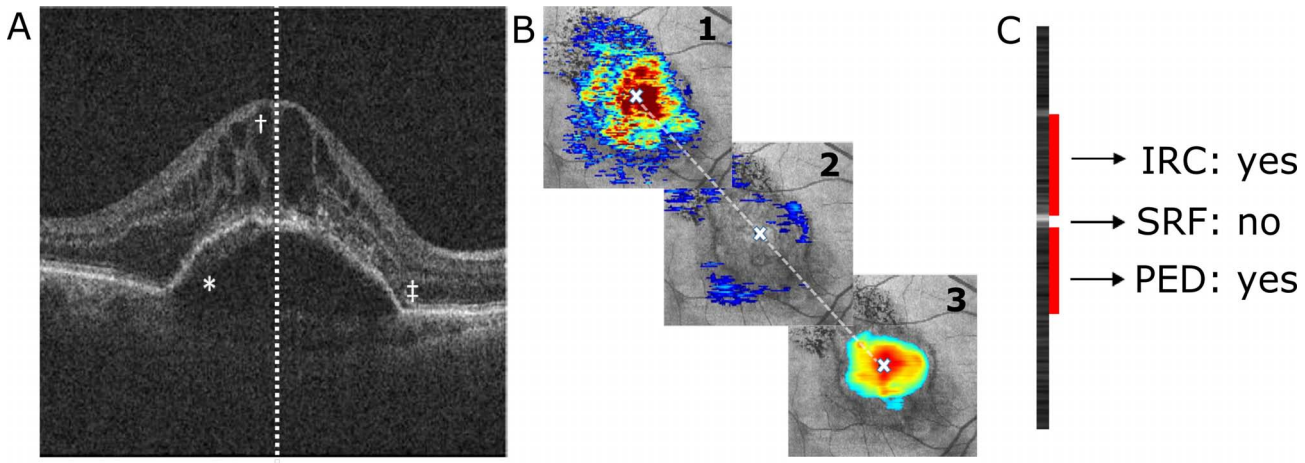

FIGURE 1. Assessment of spatial correspondence. (**A**) OCT B-scan presenting with IRC (*), SRF (†), and PED (‡). Sample A-scan location indicated by dashed line. (**B**) IRC- (1), SRF- (2), and PED- (3) en-face thickness maps. *X*s mark the sample A-scan locations, *dashed line* indicates vertical A-scan direction. (**C**) Pathomorphologic components marked in *red* alongside the sample, pixel-wide A-scan (broadened for visualization). This particular A-scan presents with IRC and PED, no SRF. In total, 61,082,112 retinal locations were analyzed according to this system.

unpaired *t*-tests performed on area measurements of IRC, SRF, and PED. The differences in performance between manual and automated segmentations were analyzed by Bland Altman plots of IRC, SRF, and PED area measurements. An α level of 0.05 was used for all statistical tests. Statistical analysis was undertaken using the SPSS version 23 statistical software package (IBM Corp., Armonk, NY, USA).

RESULTS

A total of 1341 treatment-naïve eyes of 1341 patients were eligible for inclusion. Of these, 415 eyes were imaged using Spectralis OCT, and 926 eyes were imaged using Cirrus HD-OCT. A total of 159 eyes were excluded as a result of failed automated segmentation, yielding 1182 eyes, or 119,301 automatically segmented B-scans, for the current analysis. Supplementary Tables S1 and S2 show the direct comparison of lesion disposition, spatial correspondence of lesions, and extent of area covered by pathomorphologic components between manual and automated segmentation.

Lesion Characteristics

Among automatically processed volumes, 81% presented with IRC, 95% with SRF, and 92% with PED. In the central 1-mm area, 62% of eyes presented with IRC, 59% with SRF, and 83% with PED. Descriptive data for IRC, SRF, and PED in the validation datasets (each $n = 37$) are shown in Supplementary Tables S1 and S2. Of the total 6 × 6-mm en-face-area processed by automated segmentation, a median area of 10% (IQR 3–19) was affected by SRF followed by IRC and PED, each affecting 1% and 6% of the entire area, respectively (IQR 0–3 and 3–10). In contrast, SRF was found to be the exudative component with the least extent of area within the central 1-mm field, covering a median area of 14% (IQR 3–43). The central 1-mm area was, however, intensively affected by PED with a median extension of 53% (IQR 27–74). IRC covered a median area of 18% (IQR 4–44) of the central 1 mm. The quotient of centrally affected area in relation to totally affected area was lowest in SRF with a median 1% (IQR 0–7) compared to 21 (IQR 2–41) and 19 (IQR 10–30) for IRC and PED, respectively. Cumulative distribution plots of pathomorphologic components are presented in Figure 2, showing the presence of IRC and PED being mostly restricted to the central area, while SRF seems to be distributed within most of the 6 × 6-mm area evenly throughout all patients. Supplementary Tables S1 and S2 show results obtained in manually segmented subsets, imaged by Cirrus and Spectralis, respectively. Likewise, SRF presents the pathomorphologic component with the largest extent of area in the 6 × 6-mm field.

Spatial Correspondence of Pathomorphologic Components

The median and IQR of the spatial correspondences are summarized in the Table as well as Supplementary Tables S1 and S2. The highest spatial correspondence between IRC, SRF, and PED in the 6 × 6-mm field was found among IRC-presenting scans also showing PED, at a level of median 32.9% (IQR 7–62). Vice versa, spatial correspondence of PED-affected scans including IRC was lower at a level of median 5.2% (IQR 0–22). Spatial correspondence between IRC and SRF as well as between SRF and PED was lowest, remaining below a median of 2.5%. Predominantly consistent results were obtained for the central 1-mm subfield (Table). The highest spatial correspondence appeared likewise among IRC-affected scans also showing PED, but twice as pronounced with a median 68.2% (IQR 16–100). Aside from SRF-affected scans also showing PED in median 22.4% (IQR 0–97), the spatial correspondence of IRC with SRF as well as SRF with PED showed lower proportions than in the 6 × 6-mm area. Of patients with no SRF in the central 1 mm, 32.6% also did not show IRC in the central 1 mm, whereas 67.4% presented with IRC in the central 1 mm. Regarding patients showing SRF in the central 1 mm, central IRC were absent in 41.4%, whereas 58.6% presented with IRC in the central 1 mm. A chi-square test of independence examining this relation was significant, χ^2 ($n = 1183$) = 9.57, $P < 0.01$. Per-pixel chi-square tests for SRF with PED and SRF with IRC revealed significant ORs smaller than 1 (equal log ORs < 0) in the central area, meaning that the presence of PED and IRC were less likely in areas with SRF and vice versa. Regarding the correspondence of SRF with IRC, this effect was far more pronounced in eyes scanned by Spectralis. These significant correlations occur in the center within a circle of an approximate ½-mm radius and an approximate 1-mm radius for SRF with IRC and SRF with PED, respectively. Positive correlations in the occurrence of lesions, indicated by ORs higher than 1 (equal log ORs > 0), were observed starting

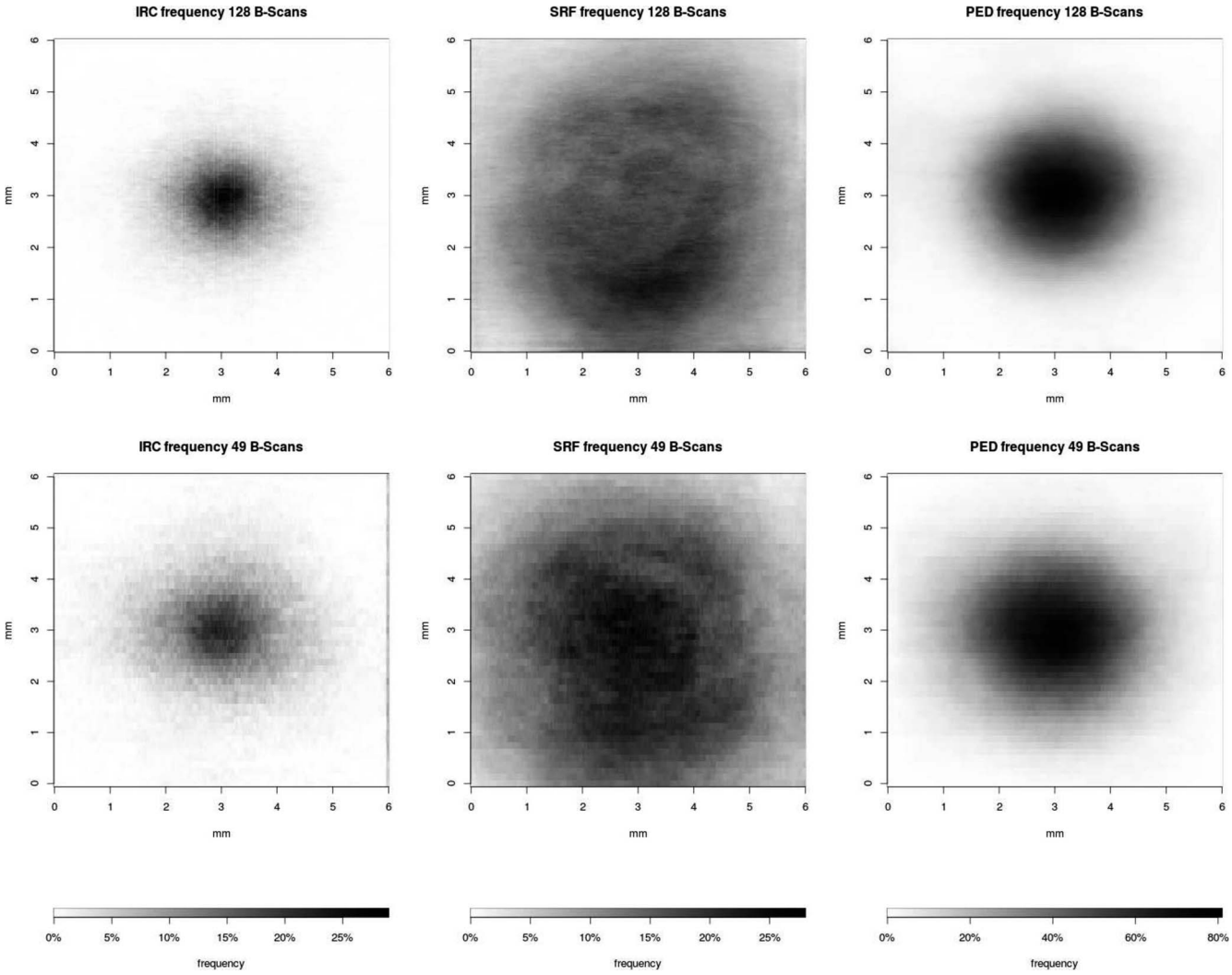

Figure 2. Cumulative distribution plots show the distribution of IRC, SRF, and PED in Cirrus (*first row*) and Spectralis (*second row*) scans. The frequency of overall per-pixel lesion coverage coded in *grayscale*. The graphs are centered on the fovea, and right eyes are mirrored to conform to left eyes.

1-mm beyond the central 1-mm area for SRF with IRC in Cirrus scans and much less pronounced in the Spectralis scans. Furthermore, the correspondence of SRF with PED revealed significant positive ORs 1.5 to 2 mm beyond the central 1-mm area in Cirrus and Spectralis scans. The correspondence between IRC and PED revealed ORs higher than 1, distributed around the center in a circle of an approximate 2-mm radius. The distribution of significant ORs throughout the 6 × 6-mm area are presented in Figure 3. Figure 4 present graphs including nonsignificant ORs. They reveal uniform trends of negative correlation of SRF with IRC and PED in the central 2-mm^2 and 3-mm^2 areas, respectively, and trends of positive correlation of SRF with IRC and PED beyond this area. The correspondence between IRC and PED shows a uniform trend of positive correlation throughout the scan. Representative patient examples including IRC-, SRF-, and PED-en-face maps are provided in Figure 5. The supplementary video shows a three-dimensional rendering of typical arrangement of the

Table. Spatial Correspondence of Pathomorphologic Components

	6 × 6-mm Area, %			1 × 1-mm Area, %		
Corresponding Pathomorphologic Components	***n***	**Md**	**IQR**	***n***	**Md**	**IQR**
Intraretinal cystoid fluid - subretinal fluid	901	2.5	0–20	691	0.0	0–9
Intraretinal cystoid fluid - RPE detachment	892	32.9	7–62	694	68.2	17–100
Subretinal fluid - intraretinal cystoid fluid	901	0.3	0–3	538	0.0	0–28
Subretinal fluid - RPE detachment	1045	1.4	0–8	635	22.4	0–97
RPE detachment - intraretinal cystoid fluid	892	5.2	0–22	802	9.0	0–49
RPE detachment - subretinal fluid	1045	2.0	0–9	943	0.0	0–10

Descriptive statistics refer to percentage of A-scans of the first pathomorphologic component covered by those of second. Md indicates median.

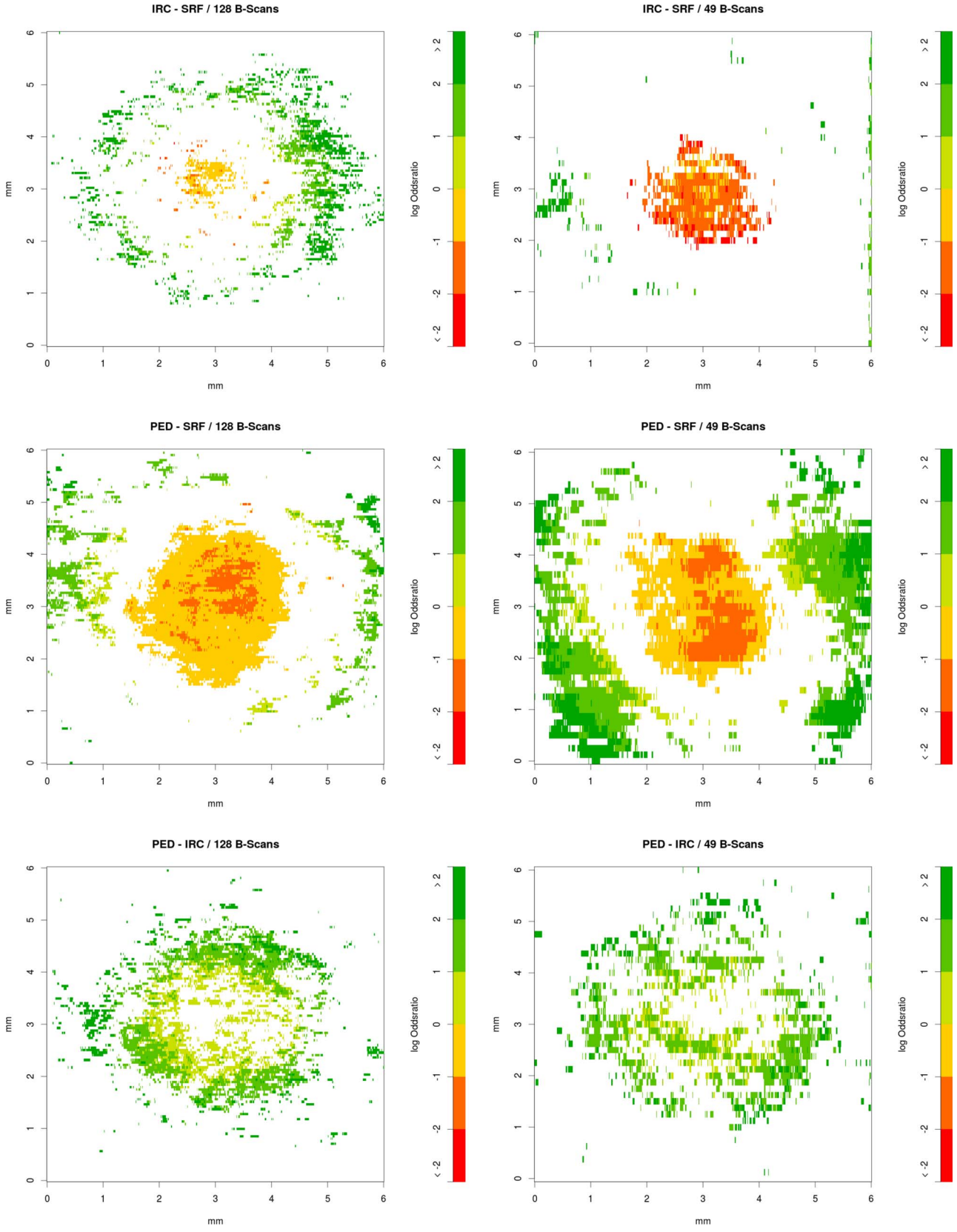

Figure 3. The plots show areas with significant relationships between features (tested with chi-square test at $\alpha = 0.05$) in Cirrus (*left column*) and Spectralis (*right column*) scans; positive correlations (log odds ratio > 0) are colored in *light green* to *dark green*, and dissociation (log odds ratio < 0) in *yellow* to *red*. The graphs are centered on the fovea, and right eyes are mirrorred to conform to left eyes.

Investigative Ophthalmology & Visual Science

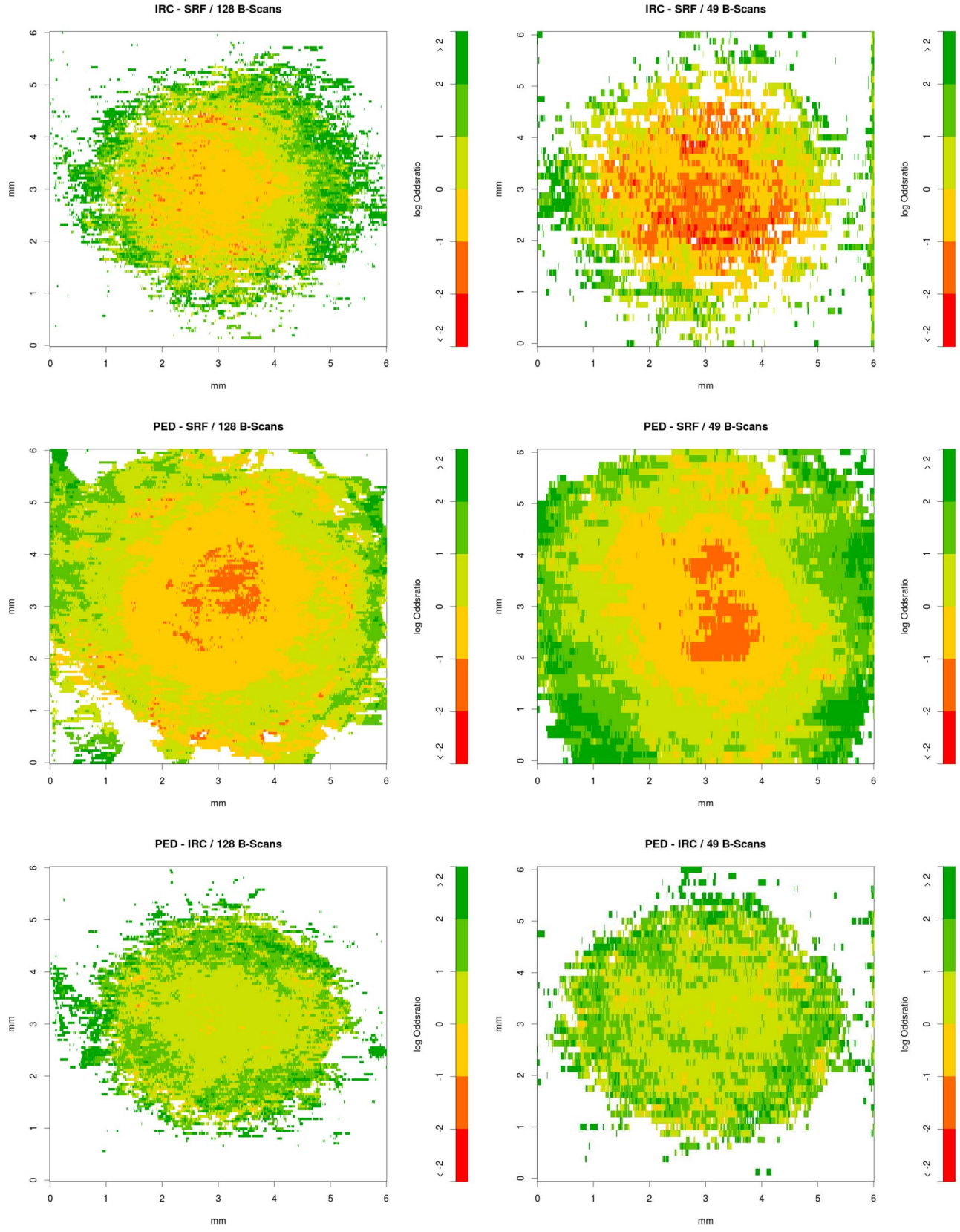

Figure 4. The plots show all areas with positive correlations between features (log odds ratio > 0) in *light green* to *dark green*, and dissociation (log odds ratio < 0) in *yellow* to *red*. No color was applied if the log odds ratio could not be calculated as a result of zero observations in one of the fields of the frequency table. The graphs are centered on the fovea, and right eyes are mirrored to conform to left eyes.

Investigative Ophthalmology & Visual Science

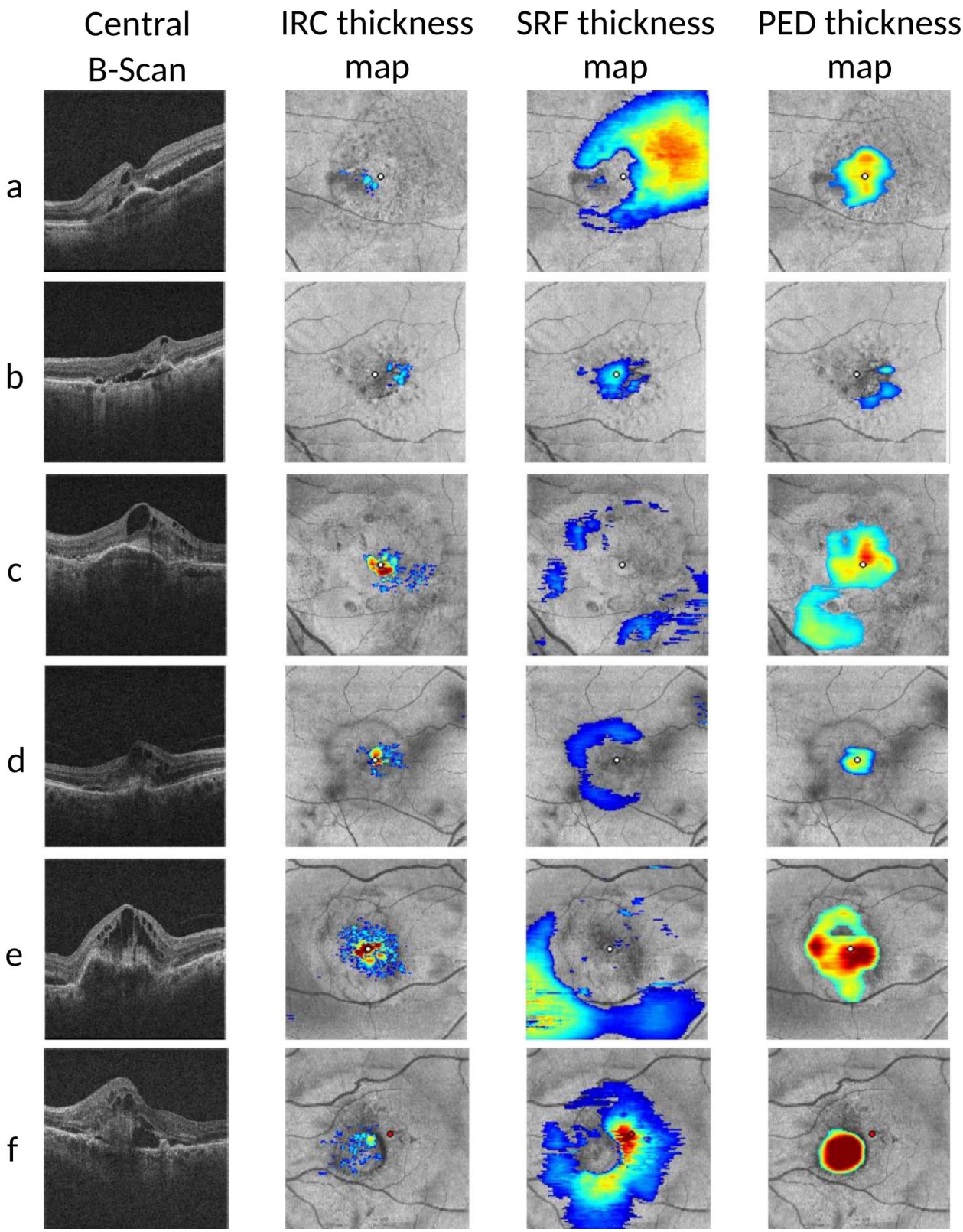

FIGURE 5. Central B-scan and corresponding IRC-, SRF-, and PED-en-face thickness maps of automatically (**a–e**) and manually (**f**) segmented example cases. Note how IRC mainly colocalize to PED lesions, whereas SRF is mainly localized in retinal locations outside PED- and IRC-affected areas.

Investigative Ophthalmology & Visual Science

individual fluid components in a study eye presenting with IRC, SRF, and PED (Supplementary Video S1). Results of IRC, SRF, and PED area measurements were tested for differences between patients imaged by Spectralis and patients imaged by Cirrus. For SRF and PED, significant differences ($P = 0.02$, $P < 0.01$, respectively) were obtained. The differences of medians however did not exceed 2% of the 6 × 6-mm area (Supplementary Fig. S1).

Supplementary Tables S1 and S2 show the direct comparison of manually and automatically obtained results. The results of spatial correspondence show less difference between segmentations in patients imaged by Spectralis. In manually segmented Cirrus images, the proportion of IRC- as well as SRF-affected A-scans also showing PED is pronouncedly lower than in automated segmentation. No further meaningful differences were observed. Bland Altman plots, illustrating the difference in IRC, SRF, and PED areas obtained by manual and automated segmentation are provided in Supplementary Figure S2.

Discussion

Identification of robust and sensitive imaging biomarkers for disease classification and treatment guidance has become a relevant focus of research in macular disease. Several studies have addressed the influence of the characteristic CNV-associated fluid compartments on visual outcome in nAMD.[7–9,12] In these reports, IRC is strongly liked with lower visual acuity (VA) at baseline as well as during anti-VEGF therapy.[7–9] By contrast, SRF has been repeatedly shown to be associated with better visual outcomes as well as stable VA results even when using an infrequent treatment regimen.[5,9,17] Furthermore, improvement in retinal sensitivity during anti-VEGF treatment has been shown to be most pronounced for SRF and serous PED, whereas patients with intraretinal fluid, particularly IRC, featured functional benefits to a lesser extent.[18] These results indicate that SRF might be an indicator of a more benign primary disease condition in nAMD. The major issue about the impact of leakage components is, however, the fact that most lesions include several fluid components at various, often confluent, locations and structure/function correlation is difficult to perform.

Potential mechanisms for an association between SRF and better VA have been described by various investigators. The outer retinal layers in patients presenting with SRF have shown to be damaged less extensively than those in patients with IRC.[11] Recently, SRF has further been associated with higher rates of photoreceptor integrity in patients with diabetic macular edema and central retinal vein occlusion (Philip A-M, et al. *IOVS* 2016;57:ARVO E-Abstract 4164). Furthermore, a reduced risk of the development of RPE atrophy has been discussed as a causative factor.[7,19,20] Freund et al.[21] consider type I neovascularization with SRF as its predominant form of fluid manifestation as a more benign subtype of CNV in nAMD. Furthermore, they hypothesize that type I neovascularization constitutes a vascular response pattern that may provide nutrients and oxygen to overlying photoreceptors thus preventing RPE and photoreceptor atrophy.[21] Also, SRF itself might supply nutrients and growth factors to adjacent structures. None of the attempts to explain the differential contribution and interaction of lesion components have so far exploited the wealth of spatial information contained in large-scale OCT data and the potential of automated segmentation. Our study demonstrated that between PED and SRF, SRF appears to less frequently present colocalized IRC. We may, therefore, hypothesize that SRF potentially acts as a spatially protective factor against vision-deteriorating IRC, whereas PED may lead to IRC with progressive visual loss.[17] Whether SRF itself or different underlying disease mechanisms tend to prevent the concomitant presence of IRC remains to be investigated.

The results of our study may allow us to hypothesize about the primary pathophysiology of disease in nAMD. Once the primary CNV lesion (most often presenting as PED) penetrates the RPE monolayer and starts to invade the neurosensory retina, proliferative and inflammatory processes may lead to a permanent adhesion between the RPE and the neurosensory tissue at the site of ingrowth. We may hypothesize that any fluid leaking from the CNV lesion will most likely pool at a locus minoris resistentiae, which, consequently, is the subretinal space around the PED lesion (Fig. 5). In contrast, we further may speculate that at the site of neovascular invasion and adhesion between the RPE and neurosensory retina, fluid pooling will most likely occur intraretinally because the retina and RPE cannot be separated easily. This mechanism of disease may be the reason of the spatial dissociation between SRF and PED/IRC and the close association between IRC and PED. Indeed, areas covered by SRF showed only very little chances of being simultaneously affected by IRC or PED. In contrast, we found IRC to often occur above primary CNV lesions, which foremost comprise PED and subretinal hyperreflective material (Fig. 5). However, in this study fluorescein angiography or indocyanine green angiography was not performed to identify the exact site of CNV. An even higher spatial correspondence of IRC and PED was observed in the central fovea. Vice-versa correspondence of PED and IRC was found to be lower, which can be attributed to the morphologic characteristics of respective components: whereas the total IRC area is made up of numerous little fluid pockets, PED is a continuous structure, which accordingly also presents below retinal tissue unaffected by IRC. In the central area, all reported observations were clearly shown to exceed effects of spatial correlation/dissociation due to the inherent distribution characteristics of each pathomorphologic feature, showing significant ORs < 1 for SRF with IRC and PED and ORs > 1 for IRC with PED. We may speculate that the effect of positive correlation of SRF with IRC and PED in the outer regions of the 6 × 6-mm area results from a combination of patients with little pathology, presenting neither feature, and severe cases, where pathology extends throughout the periphery of the scan. To substantiate this hypothesis, we show cumulative distribution plots broken down according to quartiles of lesion extent in Supplementary Figure S3. The results show the frequency of lesion occurrence to extend from central toward outward areas with growing extent of the pathomorphologic lesions. This effect seems to be most pronounced for SRF.

The results of our study, showing spatial dissociation of SRF with IRC, more precisely suggest that IRC is more frequently located extrafoveally when subfoveal SRF is present compared to when subfoveal SRF is absent. Figure 5b illustrates an example of this constellation. Thus, we may hypothesize, that the presence of subfoveal SRF possibly excludes neovascular proliferation originating from the sub-RPE space in the same area and therefore acts protectively on visual function. Considering numerous studies which have shown a negative effect of IRC and a positive effect of SRF on VA,[5,8,9,17] our findings provide a possible explanation for this phenomenon. Our concept is supported by a recent post-hoc analysis of the Comparison of AMD Treatments Trial, where subfoveal SRF was associated with better VA than extrafoveal or no SRF.[7] However, our study indicates that SRF is the exudative component least often observed in the central 1 mm (in 59% of patients compared to 62% for IRC and 83% for PED) as well as to a low extent (14% median coverage) if present. As the Comparison of AMD Treatments Trial data showed that VA in eyes with extrafoveal SRF was still higher

than in eyes with no SRF,[7] the seemingly protective role of SRF cannot solely be explained by spatial dissociation of SRF with IRC.

In our study, we performed fully automated, three-dimensional segmentation of the pathomorphologic CNV components based on graph-theoretic algorithms and convolutional neural networks, a deep-learning approach from the field of artificial intelligence that is now increasingly used in medical imaging.[14,22] The availability of reliable automated segmentation algorithms allowed us to fully exploit the three-dimensional information contained in state-of-the-art OCT volumes, where manual analysis by a clinician or a conventional reading center becomes less and less feasible. The results obtained from 1182 automatically analyzed eyes reflected those of the two subgroups including 37 eyes each in which pathologies were manually delineated.

A limitation of this study is the retrospective design, which, however, does not entail relevant drawbacks for a morphological analysis. Furthermore, the lack of use of axial and volume information of pathomorphologic components obtainable from OCT images presents a limitation. Previous reports investigating quantitative biomarkers in OCT, however, have demonstrated increased significance of SRF or IRC width compared to their axial dimension, for example, height or volume.[6,7] Cases with a tilted retina possibly introduced errors concerning actual axial spatial correspondence as the A-scan direction did not correspond to the true vertical plane perpendicular to the RPE (Fig. 5a). Possible segmentation errors produced by the fully automated three-dimensional segmentation pose a further limitation. Our data suggest a bias toward larger automated PED measurements in Cirrus scans (compared to manual measurements) and a trend to lower automated PED measurements with increasing lesion size. However, no further trends in the discrepancy between automated and manual segmentation were observed and the overall agreement between manual and automated area measurements was good (Supplementary Fig. S2). In this report we apply an innovative analysis procedure enabling highly quantitative evaluation of OCT images to OCT imaging data of a large number of patients and obtain detailed results in line with existing literature.

In conclusion, this cross-sectional study using fully automated computational analysis of more than 60 million retinal locations in 1182 eyes with treatment-naïve nAMD shows a spatial dissociation of SRF with IRC and PED in contrast to a colocalization of IRC with PED. Our findings provide further insight into the pathophysiology of the primary disease condition in AMD and may support the identification of imaging biomarkers in anti-VEGF therapy using advanced image analysis tools.

Acknowledgments

The authors thank the Austrian Federal Ministry of Science, Research and Economy and the National Foundation for Research, Technology and Development for support.

Supported by the Austrian Federal Ministry of Science, Research and Economy and the National Foundation for Research, Technology and Development. The funding organizations had no role in the design or conduct of the study.

Disclosure: **S. Klimscha**, None; **S.M. Waldstein**, Bayer Healthcare (C), Novartis (C), P; **T. Schlegl**, P; **H. Bogunović**, None; **A. Sadeghipour**, None; **A.-M. Philip**, None; **D. Podkowinski**, None; **E. Pablik**, None; **L. Zhang**, None; **M.D. Abramoff**, IDx (I), P; **M. Sonka**, P; **B.S. Gerendas**, P; **U. Schmidt-Erfurth**, Bayer Healthcare (C), Novartis (C), Alcon (C), Boehringer Ingelheim (C), P

References

1. Wong WL, Su X, Li X, et al. Global prevalence of age-related macular degeneration and disease burden projection for 2020 and 2040: a systematic review and meta-analysis. *Lancet Glob Health*. 2014;2:e106–e116.
2. Kanagasingam Y, Bhuiyan A, Abramoff MD, Smith RT, Goldschmidt L, Wong TY. Progress on retinal image analysis for age related macular degeneration. *Prog Retin Eye Res*. 2014;38:20–42.
3. Schmidt-Erfurth U, Chong V, Loewenstein A, et al. Guidelines for the management of neovascular age-related macular degeneration by the European Society of Retina Specialists (EURETINA). *Br J Ophthalmol*. 2014;98:1144–1167.
4. Schmidt-Erfurth U, Waldstein SM. A paradigm shift in imaging biomarkers in neovascular age-related macular degeneration. *Prog Retin Eye Res*. 2016;50:1–24.
5. Jaffe GJ, Martin DF, Toth CA, et al. Macular morphology and visual acuity in the comparison of age-related macular degeneration treatments trials. *Ophthalmology*. 2013;120:1860–1870.
6. Segal O, Barayev E, Nemet AY, Mimouni M. Predicting response of exudative age-related macular degeneration to bevacizumab based on spectralis optical coherence tomography. *Retina*. 2016;36:259–263.
7. Sharma S, Toth CA, Daniel E, et al. Macular morphology and visual acuity in the second year of the comparison of age-related macular degeneration treatments trials. *Ophthalmology*. 2016;123:865–875.
8. Simader C, Ritter M, Bolz M, et al. Morphologic parameters relevant for visual outcome during anti-angiogenic therapy of neovascular age-related macular degeneration. *Ophthalmology*. 2014;121:1237–1245.
9. Waldstein SM, Wright J, Warburton J, Margaron P, Simader C, Schmidt-Erfurth U. Predictive value of retinal morphology for visual acuity outcomes of different ranibizumab treatment regimens for neovascular AMD. *Ophthalmology*. 2016;123:60–69.
10. Gianniou C, Dirani A, Jang L, Mantel I. Refractory intraretinal or subretinal fluid in neovascular age-related macular degeneration treated with intavitreal ranibizumab: functional and structural outcome. *Retina*. 2015;35:1195–1201.
11. Sato T, Suzuki M, Ooto S, Spaide RF. Multimodal imaging findings and multimodal vision testing in neovascular age-related macular degeneration. *Retina*. 2015;35:1292–1302.
12. Waldstein SM, Philip AM, Leitner R, et al. Correlation of 3-dimensionally quantified intraretinal and subretinal fluid with visual acuity in neovascular age-related macular degeneration. *JAMA Ophthalmol*. 2016;134:182–190.
13. Garvin MK, Abramoff MD, Wu X, Russell SR, Burns TL, Sonka M. Automated 3-D intraretinal layer segmentation of macular spectral-domain optical coherence tomography images. *IEEE Trans Med Imaging*. 2009;28:1436–1447.
14. Schlegl T, Waldstein SM, Vogl WD, Schmidt-Erfurth U, Langs G. Predicting semantic descriptions from medical images with convolutional neural networks. *Inf Process Med Imaging*. 2015;24:437–448.
15. Lee K, Niemeijer M, Garvin MK, Kwon YH, Sonka M, Abramoff MD. Segmentation of the optic disc in 3-D OCT scans of the optic nerve head. *IEEE Trans Med Imaging*. 2010;29:159–168.
16. Zhang L, Sonka M, Folk JC, Russell SR, Abramoff MD. Quantifying disrupted outer retinal-subretinal layer in SD-OCT images in choroidal neovascularization. *Invest Ophthalmol Vis Sci*. 2014;55:2329–2335.
17. Schmidt-Erfurth U, Waldstein SM, Deak GG, Kundi M, Simader C. Pigment epithelial detachment followed by retinal cystoid degeneration leads to vision loss in treatment of neovascular

age-related macular degeneration. *Ophthalmology*. 2015;122: 822–832.

18. Sulzbacher F, Roberts P, Munk MR, et al. Relationship of retinal morphology and retinal sensitivity in the treatment of neovascular age-related macular degeneration using aflibercept. *Invest Ophthalmol Vis Sci*. 2015;56:1158–1167.
19. Engelbert M, Zweifel SA, Freund KB. Long-term follow-up for type 1 (subretinal pigment epithelium) neovascularization using a modified "treat and extend" dosing regimen of intravitreal antivascular endothelial growth factor therapy. *Retina*. 2010;30:1368–1375.
20. Sadda ST, Ding B, Hopkins JJ. Development of atrophy in neovascular AMD treated with anti-VEGF therapy: results of the HARBOR study. Paper presented at: American Academy of Ophthalmology Annual Meeting, Retina 2014 Subspecialty Day, Chicago, Illinois, USA, October 17–18, 2014.
21. Freund KB, Zweifel SA, Engelbert M. Do we need a new classification for choroidal neovascularization in age-related macular degeneration? *Retina*. 2010;30:1333–1349.
22. Deo RC. Machine learning in medicine. *Circulation*. 2015; 132:1920–1930.

Investigative Ophthalmology & Visual Science